Copyright © 2003 Tech Science Press CMES, vol.4, no.5, pp.551-557, 2003

Molecular-Dynamics Analysis of Grain-Boundary Grooving in Interconnect Films with Underlayers

T. Iwasaki[1] **and H. Miura**[1]

Abstract: We have developed a molecular-dynamics technique for investigating migration-induced failures in interconnect films for ULSIs. This technique was used to simulate grain-boundary grooving in Al and Cu films. The simulations showed that the grain-boundary grooves are formed by atomic diffusion at the grain boundary. To clarify what kind of underlay material is effective in suppressing this diffusion, we calculated the dependence of groove depth on the kind of underlay material. The calculation showed that the groove depth of the Al film decreases in the order: Al/Ta, Al/W, and Al/TiN while that of the Cu film decreases in the order: Cu/TiN, Cu/Ta, and Cu/W. The adhesion strength of interface between the interconnect film and the underlay material increases in the same order as the groove depth decreases. It is thus concluded that underlayer materials with strong adhesion to the interconnect films are effective in suppressing diffusion and grain-boundary grooving.

keyword: molecular dynamics, migration, adhesion.

1 Introduction

Migration-induced failure in thin-film interconnects is one of the major problems to be solved in order to improve device reliability of ULSIs. Such migration is usually classified as electromigration, stress migration, or thermal migration. In this study, we focused on thermal migration. Grain-boundary grooving due to diffusion (shown in Fig. 1) is a typical kind of thermal migration [Kitamura, Ohtani, and Yamanaka (1993)]. Conventionally, titanium nitride and titanium are known to be commonly used as underlayer materials for preventing the migration of Al interconnects [for example, Onoda, Kageyama, and Hashimoto (1995), and Etsabil, Rathore, and Levine (1991)]. However, such an effective underlay material has only been found by experimental trial and error; there has been no theoretical explanation of how the underlayer reduces the diffusion that causes the groove formation at grain boundaries in thin films. The authors have therefore developed a molecular-dynamics technique [Nishimura and Miyazaki (2001), and Li and Yip (2002)] that simulates grain-boundary grooving and diffusion in thin films. This technique was used to analyze the effect of underlayers on groove formation and diffusion. Accordingly, an appropriate underlayer material for reducing grain-boundary grooving and diffusion in interconnect films (Al and Cu) with underlayers (TiN, W, and Ta) could be found. The relationship between adhesion strength and groove formation was also clarified.

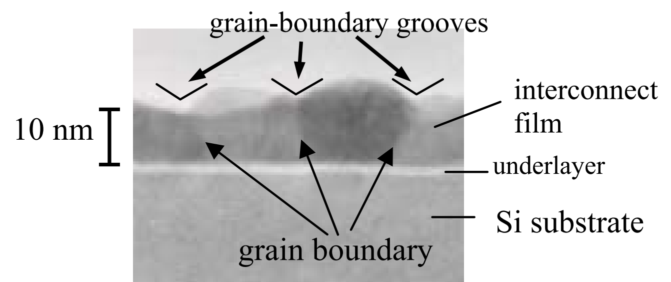

Figure 1 : Grain-boundary grooves formed at 700 K

2 Model and method of analysis

2.1 Analysis model

A bicrystal interconnect film on a bicrystal underlayer (Fig. 2) was used to study grain-boundary grooving and diffusion. Two interconnect materials (Al and Cu) and three underlayer materials (TiN, W, and Ta) were used. Both interconnect materials (Al and Cu) have the face-centered cubic (fcc) structure. Among the three kinds of underlay materials used, W and Ta have the bcc structure, and TiN has the NaCl structure. The bicrystal interconnect films with the fcc structure contain [001](310) Σ=5 tilt grain boundaries. The bicrystal underlayers

[1] Hitachi, Ltd., Tsuchiura, Ibaraki, Japan

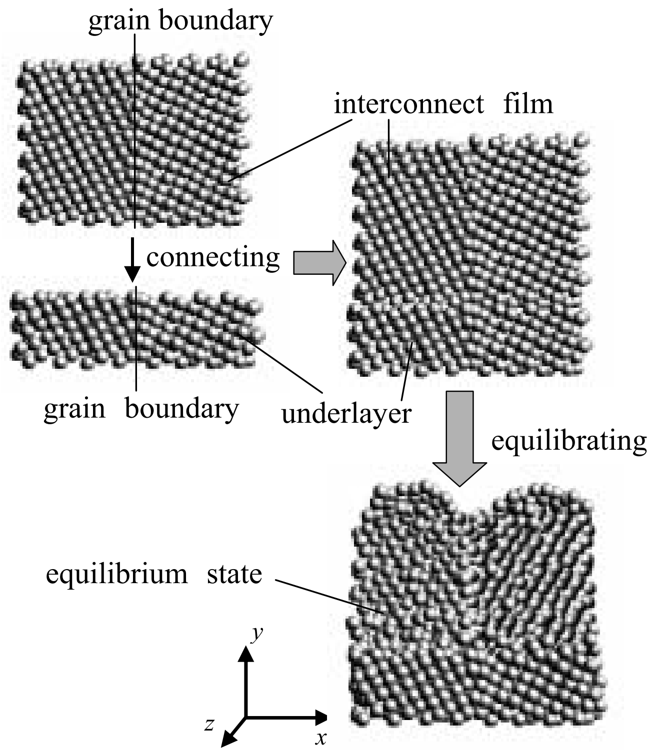

Figure 2 : Analysis model

with the NaCl structure contain [001](310) Σ=5 tilt grain boundaries while those with the bcc structure contain [001](210) Σ=5 tilt grain boundaries. The top layer of atoms were free to move while the bottom layer of atoms were fixed. The periodic boundary conditions were applied in the x and z directions. The computation cell has four atomic layers in the z direction. Before we connected the interconnect film with the underlayer, the atoms of the interconnect film and the underlayer were positioned at the bulk lattice points of their bicrystal phases. The author simulated the rearrangement of the atoms by connecting the interconnect film with the underlayer.

2.2 *Method for analyzing grain-boundary grooving and diffusion*

The basic equation used in the developed simulation technique is Newton's equation of motion,

$$m_i \mathrm{d}^2\boldsymbol{r}_i/\mathrm{d}t^2 = \partial U_T/\partial \boldsymbol{r}_i, \tag{1}$$

where m_i and $\boldsymbol{r}_i$ are the atomic mass and atomic position of the i-th atom. Total potential energy U_T is given by

$$U_T = \sum_{i<j} u_{ij} + \sum_i \phi_i\ , \tag{2}$$

where u_{ij} is the interatomic potential between the i-th and j-th atoms and ϕ_i is the potential energy of the i-th atom itself. The simulation technique uses the extended Tersoff-type potential [Yasukawa (1996)]. This potential function is shown in the Appendix. Equation (1) was numerically solved by using the Verlet algorithm [Heermann (1989)] with a time-step increment h of 1.0×10^{-15} s. The temperature was kept constant by using a scaling method [Woodcock (1971)].

By simulating the rearrangement of atoms after connecting the interconnect film with the underlayer, we investigated the groove formation at grain boundaries. The grain-boundary diffusion coefficient was calculated in order to investigate the relationship between the diffusion coefficient and the groove formation. The grain-boundary diffusion coefficient D for the interconnect film was calculated by using the following Einstein relation:

$$D = \lim_{t\to\infty} D\,(t), \tag{3}$$

$$D(t) = <[\boldsymbol{r}_i(t+t_0) - \boldsymbol{r}_i(t_0)]^2>/6t. \tag{4}$$

Here, $\boldsymbol{r}_i(t+t_0) - \boldsymbol{r}_i(t_0)$ represents the displacement of the i-th atom from time t_0 to $t+t_0$. In this study the bracket $<>$ in Eq. (4) indicates the average over two layers of atoms near the grain boundary in the interconnect film. Before we connected the interconnect film with the underlayer, the atoms of the interconnect film and the underlayer were positioned at the bulk lattice points of their bicrystal phases. After we connected the interconnect film with the underlayer at Step 1, the potential energy of the interconnect film varied widely over the earlier time steps (Fig. 3). To calculate the grain-boundary diffusion coefficient,t_0 should be set at some time in equilibrium, in which the variation of the potential energy is small. The system reached equilibrium by step 1,500, as shown in Fig. 3. We thus set t_0 in Eq. (4) to 1,500. Examples of time evolution of $D(t)$ in Eq. (4) with this value oft_0 are shown in Fig. 4. Figure 4 shows that $D(t)$ for the Al/underlayer structure converged by step 8,000. The value of$D(t)$ at step 8,000 was therefore used as the grain-boundary diffusion coefficient D. Because $D(t)$ consists of the mean-square displacement [Eq. (4)], D describes how easy it is for atoms to move and how easy it is for grooves to form. Accordingly, the author investigated what kind of underlay material is effective for making D small.

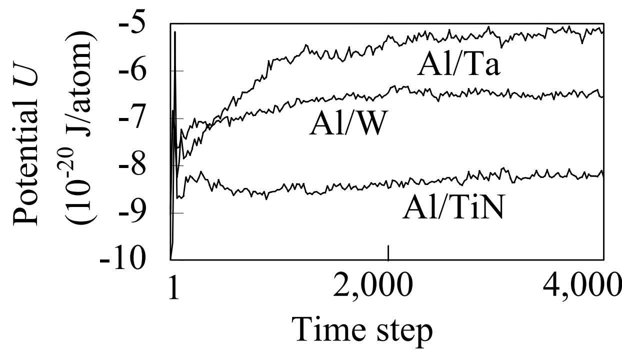

Figure 3 : Examples of time evolution of potential energy

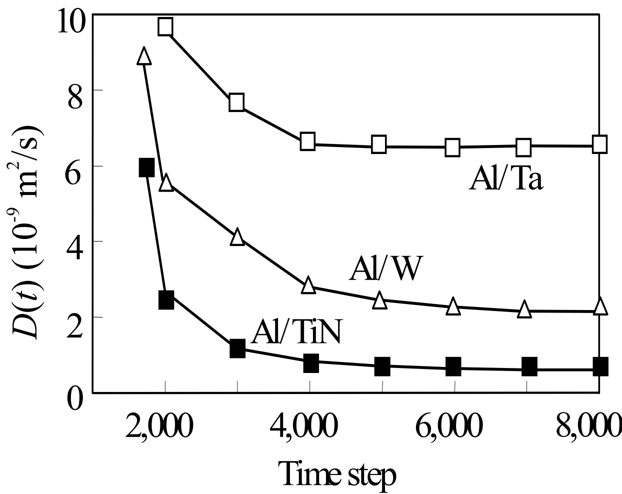

Figure 4 : Examples of time evolution of function $D(t)$

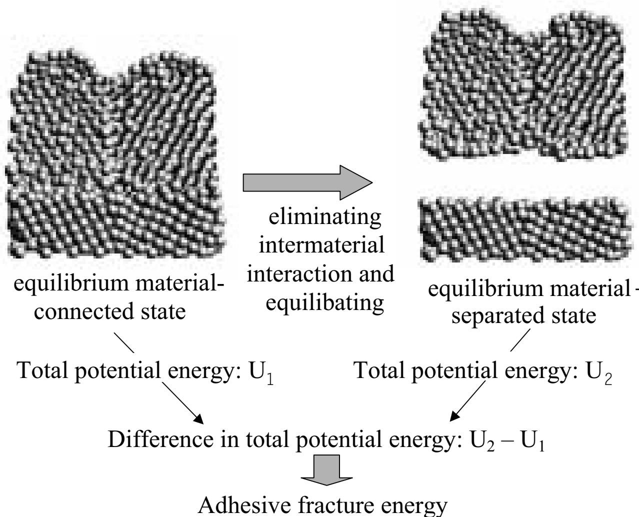

Figure 5 : Analysis model of adhesion strength

2.3 Method of adhesion analysis

To clarify the relationship between adhesion strength and groove formation, we calculated the adhesive fracture energy. We defined the adhesive fracture energy as the difference between the total potential energy of the material-connected state and that of the material-separated state (Fig. 5). The system at Step 8,000, which was in equilibrium, was used as the material-connected state. The material-separated state was obtained by eliminating the interatomic potentials between the interconnect film and the underlayer in the material-connected state and by equilibrating each film. Adhesive fracture energy V is defined as the difference between the total potential energy of the material-connected state and that of the material-separated state as follows:

$$V = \Sigma_{i<j} u_{ij} \ |_{separated} - \Sigma_{i<j} u_{ij} \ |_{connected} + \Sigma_i \phi_i|_{separated} - \Sigma_i \phi_i|_{connected}. \quad (5)$$

The first term on the right-hand side of Eq. (5) is the sum of u_{ij} over all pairs of atoms. On the other hand, the second term on the right-hand side of Eq. (5) does not include the sum over pairs of interconnect and underlayer atoms because the intermaterial interaction between the interconnect and the underlay materials is not included in the material-separated state. We calculated the adhesive fracture energies V of the interfaces between the interconnect films (Al and Cu) and the underlayers (TiN, W, and Ta).

3 Analysis results

3.1 Results on grain-boundary grooving and diffusion

The atomic configurations at step 8,000 obtained at T =700 K are shown in Figs. 6 and 7, which show the profiles of grain-boundary grooves in Al and Cu films on underlayers, respectively. The depth of the grooves in the Al film decreases in the order: Al/Ta, Al/W, and Al/TiN, while that in the Cu film decreases in the order: Cu/TiN, Cu/Ta, and Cu/W. The depth for the Al/TiN structure is the smallest of all. This result is consistent with the fact that TiN and Ti are commonly used as underlay materials to prevent the migration of Al interconnects [for example, Onoda, Kageyama, and Hashimoto (1995), and Etsabil, Rathore, and Levine (1991)].

The grain-boundary diffusion coefficients of the Al and Cu films calculated at T =700 K are shown in Figs. 8

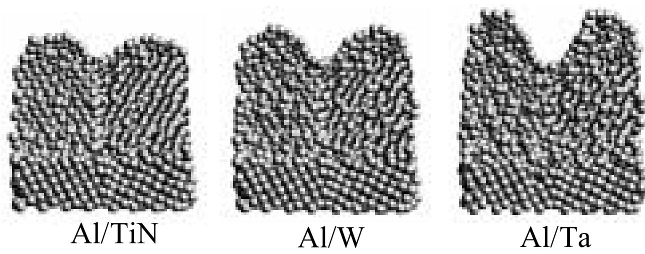

Figure 6 : Groove profiles in Al films on underlayers

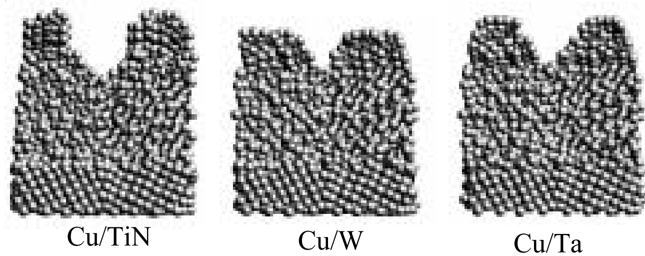

Figure 7 : Groove progiles in Cu films on underlayers

and 9, respectively. The grain-boundary diffusion coefficient of the Al film decreases in the order: Al/Ta, Al/W, and Al/TiN, while that of the Cu film decreases in the order: Cu/TiN, Cu/Ta, and Cu/W. Therefore, it can be said that the grain-boundary diffusion coefficient decreases in the same order as the depth of the grain-boundary groove decreases. This result shows that the groove formation is caused by grain-boundary diffusion.

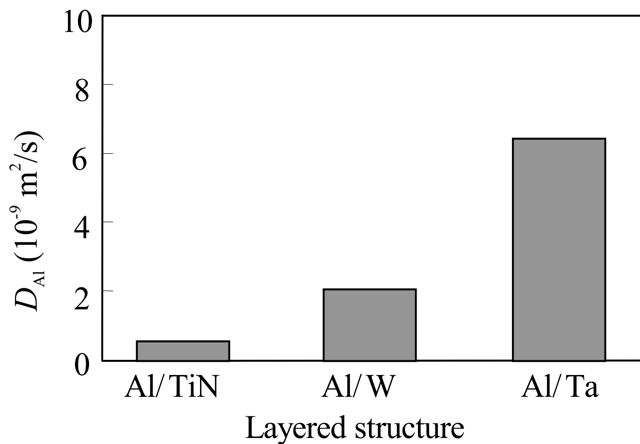

Figure 8 : Grain-boundary diffusion coefficient of Al

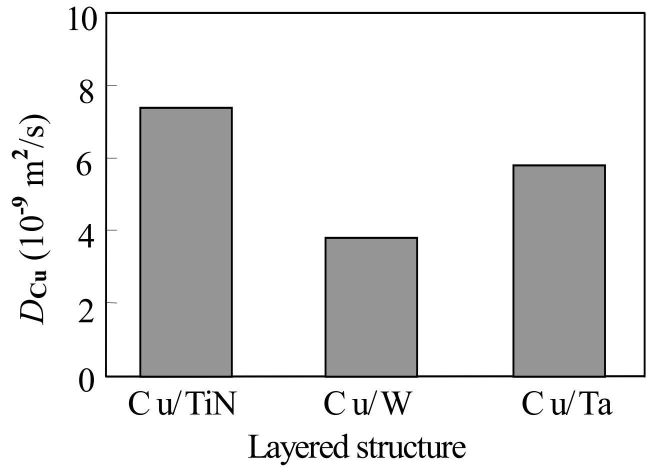

Figure 9 : Grain-boundary diffusion coefficient of Cu

3.2 *Results for adhesion strength*

The adhesion strength of the Al and Cu films calculated from molecular dynamics are shown in Figs. 10 and 11, respectively. The adhesion strength of the Al film increases in the order: Al/Ta, Al/W, and Al/TiN while that of the Cu film increases in the order: Cu/TiN, Cu/Ta, and Cu/W. Therefore, it can be said that the adhesion strength increases in the same order as the depth of the grain-boundary groove decreases. It is thus considered that the adhesion strength is related to migration resistance as well as the grain-boundary diffusion and that using underlay materials with good adhesion to interconnect films is effective in suppressing grain-boundary grooving.

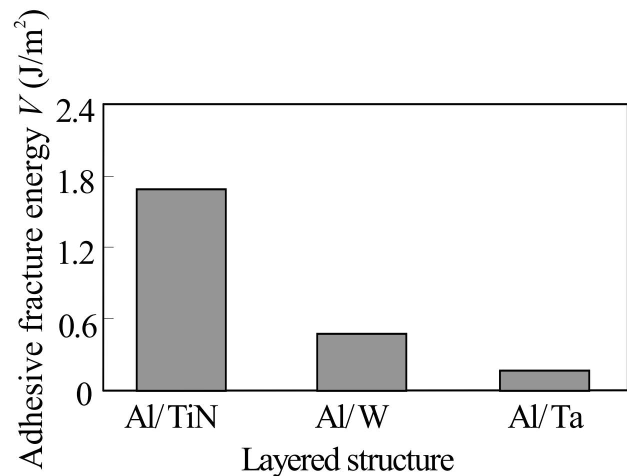

Figure 10 : Adhesion strength of Al/underlayer structure

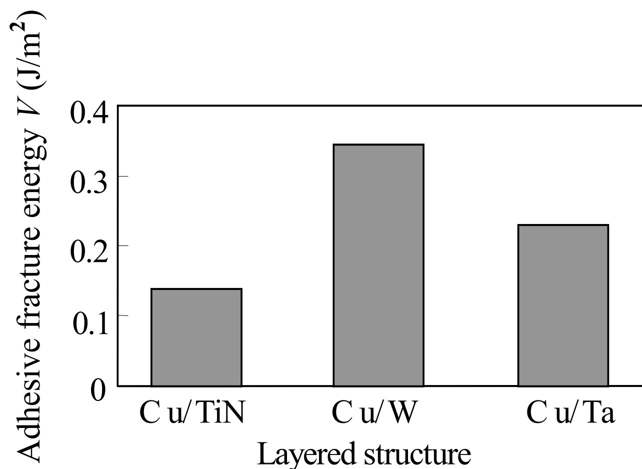

Figure 11 : Adhesion strength of Cu/underlayer structure

4 Discussions

In this study, grain-boundary grooving in interconnect films was simulated by using only an atomic-scale method. Therefore, we were able to handle only partial models for analysis (Fig. 2). To get one step further towards understanding the mechanism of migration-induced failure in thin-film interconnects, we are now trying to handle whole-device models by using a multi-scale method [for example, Srivastava and Atluri (2002), and Ghoniem and Cho (2002)]. In addition, the effects of mechanical stress on fracture patterns are considered to be important [for example, Abraham (2000), Nishimura and Miyazaki (2001), and Wei, Srivastava, and Cho (2002)]. We are studying the effects of mechanical stress on grain-boundary grooving by applying the stress to the interconnect films. The results of these studies will appear in future papers.

5 Summary

We have developed a molecular-dynamics technique for investigating migration-induced failures in interconnect films. This technique was used to simulate grain-boundary grooving in Al and Cu films. These simulations showed that the grain-boundary grooves were formed by atomic diffusion at the grain boundary. To clarify what kind of underlay material is effective in suppressing diffusion, we calculated the dependence of grain-boundary groove depth on the underlay material. The calculation showed that the groove depth of the Al film decreases in the order: Al/Ta, Al/W, and Al/TiN while that of the Cu film decreases in the order: Cu/TiN, Cu/Ta, and Cu/W. The adhesion strength of the interface between the interconnect film and the underlay material increases in the same order as the groove depth decreases. It is thus considered that underlay materials with strong adhesion to interconnect films are effective in suppressing diffusion and grain-boundary grooving.

References

Abraham, F. F. (2000): MAADLY spanning the length scales in dynamic fracture. *CMES*, Vol. 1, No. 4, pp. 63-70.

Etsabil, J. J.; Rathore, H. S.; Levine, E. N. (1991): Electromigration improvements with titanium underlay and overlay in Al(Cu) metallurgy. *Proc. of 8th IEEE VMIC*, pp. 242-248.

Ghoniem, N. M.; Cho, K. (2002): The emerging role of multiscale modeling in nano- and micro-mechanics of materials. *CMES: Computer Modeling in Engineering & Sciences*, Vol. 3, No. 2, pp. 147-174.

Heermann, W. (1989): *Computer simulation methods. Second edition*, Springer-Verlag, Berlin, pp. 13-50.

Kitamura, T.; Ohtani, R.; Yamanaka, T. (1993): Numerical simulation of stress-induced failure in aluminum conductors of a microelectronic package based on surface and grain boundary diffusion. *Transactions of the Japan Society of Mechanical Engineers*, Vol. 59, pp. 1625-1630.

Li, J.; Yip, S. (2002): Atomistic measures of materials strength. *CMES: Computer Modeling in Engineering & Sciences*, Vol. 3, No. 2, pp. 219-228.

Nishimura, K.; Miyazaki, N. (2001): Molecular dynamics simulation of crack propagation in polycrystalline material. *CMES: Computer Modeling in Engineering & Sciences*, Vol. 2, No. 2, pp. 143-154.

Onoda, H.; Kageyama, M.; Hashimoto, K. (1996): Al-Si crystallographic-orientation transition in Al-Si/TiN layered structures and electromigration performance as interconnects. *J. Appl. Phys.*, Vol. 77, pp. 885-892.

Srivastava, D.; Atluri, S. N. (2002): Computational nanotechnology: A current perspective. *CMES: Computer Modeling in Engineering & Sciences*, Vol. 3, No. 5, pp. 531-538.

Tersoff, J. (1989): Modeling solid-state chemistry: In-

teratomic potentials for multicomponent systems. *Phys. Rev.*, Vol. B39, 5566-5568.

Yasukawa, A. (1996): Using an extended Tersoff interatomic potential to analyze the static-fatigue strength of SiO_2 under atmospheric influence. *JSME International Journal*, Series A, Vol. 39, pp. 313-320.

Wei, C.; Srivastava, D.; Cho, K. (2002): Molecular dynamics study of temperature dependent plastic collapse of carbon nanotubes under axial compression. *CMES: Computer Modeling in Engineering & Sciences*, Vol. 3, No. 2, pp. 255-262.

Woodcock, L. V. (1971): Isothermal molecular dynamics calculations for liquid salts. *Chem. Phys. Lett.*, Vol. 10, pp. 257-261.

Appendix

The details of the extended Tersoff-type potentials used in this study are explained in other works [Yasukawa (1996)]. We therefore describe only an outline of the potentials. The potential functions are written as follows:

$$U_T = \sum_{i<j} u_{ij} + \sum_i \phi_i , \quad (6)$$

$$\phi_i=[(I_{Ei}+A_{Ei})/(2e)]q_i+[(I_{Ei}-A_{Ei})/(2e^2)]q_i^2, \quad (7)$$

$$u_{ij} = u_{REPij} + u_{SHTij} + u_{IONij} + u_{VDWij}, \quad (8)$$

$$u_{REPij} = f_{Sij}A_{ij}\exp(-\lambda_{ij}r_{ij}), \quad (9)$$

$$u_{SHTij}= -f_{Sij}b_{ij}B_{ij}\exp(-\mu_{ij}r_{ij}), \quad (10)$$

$$u_{IONij} = f_{Lij}\eta_i\eta_Ł q_iq_j/(4\pi\varepsilon_0 r_{ij}), \quad (11)$$

$$u_{VDWij}= -f_{Lij}(C_{VDWi}C_{VDWŁ})^{1/2}/r_{ij}^6, \quad (12)$$

$$b_{ij}= [1+(\beta_i\Sigma\zeta_{ijk})^{ni}]^{-1(2ni)}, \quad (13)$$

$$\zeta_{ijk} = f_{Sij} \exp [\mu_{ij}^{mi}(r_{ij}-r_{ik})^{mi}]\{1+c_i^2/d_i^2-c_i^2/ [d_i^2+(h_I\text{-}\cos\theta_{ijk})^2]\}, \quad (14)$$

$$f_{Sij} = f_c(r_{ij}, (R_{Si}R_{Sj})^{1/2} , (S_{Si}S_{Sj})^{1/2}), \quad (15)$$

$$f_{Lij} = f_c(r_{ij}, (R_{Li}R_{Lj})^{1/2} , (S_{sLi}S_{Lj})^{1/2}), \quad (16)$$

$$f_c (r, R , S) =1 \text{ (in the case of } R \geq r), \quad (17)$$

$$f_c (r, R , S) =1/2+(1/2)\cos[\pi(r-R) /(S-R)]$$

$$\text{(in the case of } R<r<S), \quad (18)$$

$$f_c (r, R , S) =0 \text{ (in the case of } r \geq S), \quad (19)$$

$$\lambda_{ij}=(\lambda_i+\lambda_j)/2, \quad (20)$$

$$\mu_{ij}=(\mu_i+\mu_j)/2, \quad (21)$$

$$A_{ij}= (A_{Si}A_{Sj})^{1/2}, \quad (22)$$

$$B_{ij}= (B_{Si}B_{Sj})^{1/2}, \quad (23)$$

$$A_{Si} = A_i\exp(\lambda_iD_i), \quad (24)$$

$$B_{Si} = B_i[\exp(\mu_iD_i)][a_{Bi} \text{ - } |b_{Bi}(q_I-Q_{Oi})^{nBi}], \quad (25)$$

$$D_i = D_{Ui} +|b_{Di}(Q_{Ui} - q_i) |^{nDi}, \quad (26)$$

$$b_{Di}= (D_{Li} - D_{Ui})^{1/nDi} /(Q_{Ui} - Q_{Li}), \quad (27)$$

$$n_{Di}=\{\ln[D_{Ui}/((D_{Ui}\text{-}D_{Li})]\}/\{\ln[Q_{Ui} /((Q_{Ui}\text{-}Q_{Li})]\}, \quad (28)$$

$$b_{Bi} =| a_{Bi} |^{1/nBi}/\Delta Q_i, \quad (29)$$

$$a_{Bi}= 1/(1 \text{ - } | Q_{Oi}/\Delta Q_i | ^{nBi}), \quad (30)$$

$$Q_{Oi}=(Q_{Ui}+Q_{Li})/2, \quad (31)$$

and

$$\Delta Q_i=(Q_{Ui}-Q_{Li})/2, \quad (32)$$

where U_T is total potential energy, u_{ij} is the interatomic potential between the i-th and j-th atoms, and ϕ_i is the potential energy of the i-th atom itself. $\sum_{i<j}$ is the summation over all pairs of atoms, $\sum_i$ is the summation over all atoms i, and $\sum_k$ is the summation over all atoms k except atoms i and j. The functionsu_{REPij}, u_{SHTij}, u_{IONij}, andu_{VDWij} are repulsive energy, short-range energy, ionic bond energy, and van der Waals energy, respectively. When there is no charge transfer, the terms $u_{REPij} + u_{SHTij}$ in Eq. (8) coincide with the original Tersoff potential [Tersoff (1989)]. And e is elementary charge, π is circular constant, ε_0 is the permittivity of the vacuum,r_{ij} is the distance between atoms i and j, θ_{ijk} is the angle between bonds ij and ik, andq_i is the charge of atom i. Parameter values for Cu, Al, N, Ti, W, and Ta are listed in Tables 1 and 2. The chargeq_i must be redetermined at every time step so thatU_T is minimized.

	Cu	Al	N
A (10^{-18} J)	128.5	49	584.0
B (10^{-18} J)	6.92	4.22	60.8
λ (10^{10}/m)	2.83	2.2	5.38
μ (10^{10}/m)	1.412	1.099	2.69
β	0	0	2
n	1	1	1
m	1	1	1
c	0	0	0
d	1	1	1
h	0	0	0
R_S (10^{-10} m)	2.82	3.15	1.537
S_S (10^{-10} m)	3.33	3.72	1.976
R_L (10^{-10} m)	1.1	1.1	1.1
S_L (10^{-10} m)	5.0	5.0	5.0
I_E/e (J/C)	7.72	5.98	14.53
A_E/e (J/C)	0.90	0.52	0
Q_L/e	-6	-5	-3
Q_U/e	2	3	5
D_L (10^{-10} m)	1.49	1.61	2.14
D_U (10^{-10} m)	-1.12	-1.5	-1.08
n_B	10	10	10
η	1	1	1
C_{VDW} (Jm^6)	0	0	0

Table 1 : Parameters for low-melting-point materials

	Ti	W	Ta
A (10^{-18} J)	90.4	740.0	252.0
B (10^{-18} J)	6.86	26.5	14.8
λ (10^{10}/m)	2.26	2.94	2.468
μ (10^{10}/m)	1.127	1.467	1.234
β	0	0	0
n	1	1	1
m	1	1	1
c	0	0	0
d	1	1	1
h	0	0	0
R_S (10^{-10} m)	3.16	3.56	3.72
S_S (10^{-10} m)	3.74	4.11	4.29
R_L (10^{-10} m)	1.1	1.1	1.1
S_L (10^{-10} m)	5.0	5.0	5.0
I_E/e (J/C)	6.82	7.98	7.88
A_E/e (J/C)	1.24	0	0
Q_L/e	-4	-2	-3
Q_U/e	4	6	5
D_L (10^{-10} m)	1.58	1.59	1.60
D_U (10^{-10} m)	-1.44	-1.46	-1.47
n_B	10	10	10
η	1	1	1
C_{VDW} (Jm^6)	0	0	0

Table 2 : Parameters for high-melting-point materials